# Tensorial analysis of the long-range interaction between metastable alkaline-earth atoms

Robin Santra and Chris H. Greene
*JILA, University of Colorado, Boulder, CO 80309-0440*
(Dated: June 6, 2005)

Alkaline-earth atoms in their lowest $(nsnp)\ ^3P_2$ state are exceptionally long-lived and can be trapped magnetically. The nonspherical atomic structure leads to anisotropic long-range interactions between two metastable alkaline-earth atoms. The anisotropy affects the rotational motion of the diatomic system and couples states of different rotational quantum numbers. This paper develops a tensorial decomposition of the most important long-range interaction operators, and a systematic inclusion of molecular rotations, in the presence of an external magnetic field. This analysis illuminates the nature of the coupling between the various degrees-of-freedom. The consequences are illustrated by application to a system of practical interest: metastable $^{88}$Sr. Using atomic parameters determined in a nearly-*ab initio* calculation, we compute adiabatic potential energy curves. The anisotropic interatomic interaction, in combination with the applied magnetic field, is demonstrated to induce the formation of a long-range molecular potential well. This curve correlates to two fully polarized, low-field seeking atoms in a rotational s-wave state. The coupling among molecular rotational states controls the existence of the potential well, and its properties vary as a function of magnetic-field strength, thus allowing the scattering length in this state to be tuned. The scattering length of metastable $^{88}$Sr displays a resonance at a field of 339 Gauss.

PACS numbers: 34.20.Cf, 34.20.Mq, 31.10.+z

## I. INTRODUCTION

The ability of van der Waals' equation-of-state of a real gas [1] to describe the phase transition from the gaseous to the liquid state is one of the manifestations of the universal importance that must be attributed to interatomic forces. Renewed interest in their detailed understanding has been prompted by the experimental demonstration [2, 3] of a pure quantum phase transition—Bose-Einstein condensation—in dilute gases of alkali-metal atoms. Ultracold conditions, which are necessary for the formation of a Bose-Einstein condensate, provide an ideal setting to observe, and measure precisely, weak interatomic interactions [4].

Alkali atoms constitute a natural choice: They possess strong electric dipole transitions from their ground state that lie in the visible range of the electromagnetic spectrum. This makes them ideal candidates for laser cooling techniques. Furthermore, as effective one-electron systems they have a magnetic dipole moment and can be trapped in a suitably shaped magnetic field. The experimental interest in alkali atoms triggered precision theoretical studies devoted to uncovering their long-range interaction properties [5, 6, 7, 8].

Noble-gas atoms become accessible to laser cooling if they are not in their electronic ground state but in an excited, metastable one. Dispersion coefficients for metastable helium, $2\ ^1S_0$ and $2\ ^3S_1$, have been calculated, for example, by Chen [9] and by Yan and Babb [10]. The metastable states of the heavier noble gases can be written as $\left(np^5(n+1)s\right)\ ^3P_2$ ($n = 2$ for neon, and so on). The associated electron distributions are nonspherical, in contrast to the $2\ ^1S_0$ and $2\ ^3S_1$ states of atomic He—and in contrast to ground-state alkali atoms. The interactions between such metastable noble-gas atoms are not isotropic, and they are not pure dispersion forces. (Dispersion coefficients are reported in Ref. [11].) The most important new interaction is the electric quadrupole-quadrupole interaction, as discussed by Doery *et al.* [12]. Under normal conditions, anisotropic interactions between the constituents of a gas tend to be smeared out due to thermal averaging. Only ultracold temperatures permit their detailed study.

Recently, alkaline-earth atoms have moved into the focus of interest. In their ground state they can be laser-cooled using the strong $^1S_0 \rightarrow\ ^1P_1$ transition [13, 14]. Katori *et al.* exploited the extremely narrow $^1S_0 \rightarrow\ ^3P_1$ intercombination transition to achieve laser cooling of ground-state $^{88}$Sr down to a few hundred nano-Kelvin [15]. Stable alkaline-earth isotopes with an even number of nucleons predominate, which therefore possess no nuclear magnetic moment: Their electronic spectra are free of hyperfine structure. This simplifies the interpretation of experimental data and facilitates comparison to theory [16]. The analysis of the photoassociative spectrum of cold $^{40}$Ca atoms measured by Zinner *et al.* may serve as an illustration [17].

Ground-state alkaline-earth atoms, which have a closed-shell electronic structure, do not lend themselves to pure magnetic trapping. Switching off the light field employed to hold the laser-cooled atoms in a magneto-optical trap, followed by evaporative cooling down to quantum degeneracy, is thus not an option. An interesting strategy to overcome this obstacle is to work with metastable alkaline-earth atoms in their lowest $(nsnp)\ ^3P_2$ state [18, 19], which have radiative lifetimes of the order of ten minutes [20]. The experimental feasibility of magnetic trapping of

metastable $^{88}$Sr has already been demonstrated [21, 22, 23].

Metastable alkaline-earth atoms share with metastable noble-gas atoms (excluding He) the property of interacting through anisotropic forces. However, as was shown quantitatively by Derevianko [20], the dominant electric quadrupole-quadrupole interaction is noticeably stronger among alkaline-earth atoms: Their large quadrupole moment is a consequence of the relatively diffuse spatial distribution of the excited p-electron; the lack of spherical symmetry of a metastable noble-gas atom, on the other hand, is due to the hole in the compact valence shell, shielded by an orbiting electron of s-symmetry. Since metastable alkaline-earth atoms—in contrast to noble-gas atoms—do not suffer from trap losses via the phenomenon of Penning ionization [24], they offer the exciting prospect of quantum degenerate gases with pronounced anisotropic interatomic interactions.

Derevianko and co-workers recently presented a first, simplified analysis of the ultracold collision properties of metastable alkaline-earth atoms [25]. They predict the existence of a long-range molecular potential well for the electronic state of highest Zeeman energy in a given external magnetic field. The scattering length on this potential energy curve can be tuned by adjusting the magnetic-field strength, thus enabling control of sign and strength of the effective interatomic interaction at ultracold temperatures. The numerical results in Ref. [25] are based on the assumption that s-wave scattering of two metastable alkaline-earth atoms in the low-field seeking state mentioned above is sensitive only to the rotationally invariant part of the interatomic interaction potential. However, as we shall show in this paper, that approximation is not justified in the case of relatively strong anisotropic coupling and does not lead to quantitatively accurate predictions.

In order to provide a systematic framework for describing anisotropic interactions, we present in Sec. II a detailed tensorial analysis of the leading interatomic interaction operators. In particular, we show that the electric quadrupole-quadrupole operator transforms like a spherical tensor of rank four, and we decompose the electric dipole-dipole dispersion operator into tensors of rank zero, two, and four. Similar tensorial ideas have been applied, for instance, to the anisotropic interactions between molecules [26, 27, 28] and these were crucial to formally demonstrate the surprising existence of a vector interaction—a tensorial coupling of rank one—between a high-angular momentum Rydberg electron and an anisotropic ionic core [29, 30]. General introductions to the techniques of spherical tensor algebra may be found in Refs. [31], [32], and [33].

An important new ingredient, facilitated by our use of tensorial methods, is the inclusion of the quantum-mechanical rotation of an anisotropically interacting diatomic system in a magnetic field (Sec. III). At interatomic distances of a few hundred Bohr radii, electronic interaction energies and rotational energies are comparable. Anisotropic interatomic interaction leads to coupling between different rotational quantum states, and the classification of a diatomic eigenstate using just a single rotational quantum number ceases to be meaningful.

Section IV is devoted to the discussion of a concrete example: metastable $^{88}$Sr. We have calculated all relevant long-range parameters (magnetic dipole moment, electric quadrupole moment, and dispersion coefficients), treating the correlation between the two valence electrons in atomic $^{88}$Sr fully. Using these parameters, which are in generally good agreement with the ones presented in Ref. [25], we obtain adiabatic potential curves by diagonalizing the complete diatomic Hamiltonian as a function of interatomic separation. Our calculations reproduce the phenomenon of a potential well in the low-field seeking state, correlating at large interatomic separations to a rotational s-wave state and fully polarized atoms with highest Zeeman energy. We make use of perturbation theory to shed light on how the interplay of the different physical operators generates the long-range molecular potential well. Our analysis clarifies how the magnetic-field strength affects depth and location of the potential minimum. It also shows that, at interatomic distances in the vicinity of and below the potential well minimum, the eigenstate acquires an appreciable admixture of higher rotational quantum states. Indeed, for this reason the scattering lengths we find on the basis of our numerical data differ substantially from those reported by Derevianko *et al.* [25].

A concluding discussion is given in Sec. V. We use atomic units throughout, unless otherwise noted.

## II. TENSORIAL STRUCTURE OF INTERATOMIC INTERACTION OPERATORS

### A. Leading expansion terms and Feshbach formalism

The interaction Hamiltonian, $H_{\rm int}$, of two atoms whose electron clouds do not overlap can be expanded in terms of inverse powers of the interatomic distance, $R$, by applying techniques well known from classical electrodynamics [34, 35, 36, 37]. All operators in the resulting series can be expressed using purely atomic observables.

Given a neutral atomic species with nonvanishing magnetic-dipole and electric-quadrupole moments, the leading expansion contributions up to fifth order in $1/R$ can be written as

$$H_{\rm int} = H_{\rm dd} + H_{\rm mm} + H_{\rm dq} + H_{\rm qq}, \tag{1}$$

where

$$H_{\rm dd} = \frac{1}{R^3}\sum_{i_1,i_2}\{\boldsymbol{x}_{i_1}\cdot\boldsymbol{x}_{i_2} - 3(\boldsymbol{x}_{i_1}\cdot\boldsymbol{n})(\boldsymbol{x}_{i_2}\cdot\boldsymbol{n})\} \tag{2}$$

is the familiar electric dipole-dipole interaction operator. $\boldsymbol{x}_{i_1}$ symbolizes the position of an electron belonging to atom 1 relative to the nucleus of that atom. Similarly, $\boldsymbol{x}_{i_2}$ refers to an electron in atom 2, measured in relation to the nucleus of atom 2. $\boldsymbol{n}$ denotes a unit vector along the diatomic axis. Using spherical multipole moment operators, defined as

$$q^{(k)}_{l,m} := -\sum_{i_k} r^l_{i_k} C_{l,m}(\vartheta_{i_k},\varphi_{i_k}), \tag{3}$$

$(r_{i_k},\vartheta_{i_k},\varphi_{i_k})$ representing spherical coordinates of vector $\boldsymbol{x}_{i_k}$ and $C_{l,m}(\vartheta_{i_k},\varphi_{i_k})$ being related to the spherical harmonic $Y_{l,m}(\vartheta_{i_k},\varphi_{i_k})$ through the simple relation

$$C_{l,m}(\vartheta_{i_k},\varphi_{i_k}) := \sqrt{\frac{4\pi}{2l+1}}Y_{l,m}(\vartheta_{i_k},\varphi_{i_k}), \tag{4}$$

the electric dipole-dipole operator reads

$$H_{\rm dd} = -\frac{1}{R^3}\left\{q^{(1)}_{1,+1}q^{(2)}_{1,-1} + 2q^{(1)}_{1,0}q^{(2)}_{1,0} + q^{(1)}_{1,-1}q^{(2)}_{1,+1}\right\}. \tag{5}$$

The basic assumption underlying this representation of $H_{\rm dd}$ is that the vector $\boldsymbol{n}$ introduced in Eq. (2) is identical to $\boldsymbol{e}_z$, the Cartesian unit vector along the $z$-axis of a chosen reference frame. Hence, Eq. (5), and all other equations in the remainder of this section, refer to a body-fixed frame. We will return to this point later when we incorporate the effect of molecular rotation.

The second term on the right-hand side of Eq. (1) describes the magnetic dipole-dipole interaction [38] between atom 1 and atom 2:

$$H_{\rm mm} = -\frac{1}{R^3}\left\{\mu^{(1)}_{+1}\mu^{(2)}_{-1} + 2\mu^{(1)}_{0}\mu^{(2)}_{0} + \mu^{(1)}_{-1}\mu^{(2)}_{+1}\right\}. \tag{6}$$

The magnetic dipole operator,

$$\boldsymbol{\mu}^{(k)} = -\mu_{\rm B}\left\{\boldsymbol{j}^{(k)} + \boldsymbol{s}^{(k)}\right\} \tag{7}$$

($\mu_{\rm B}$: Bohr magneton; $\boldsymbol{j}^{(k)}$: total angular momentum of atom $k$; $\boldsymbol{s}^{(k)}$: spin of atom $k$), is a spherical tensor of rank one. Since we restrict our treatment of magnetic effects to the dipole term, we suppress the rank index of $\boldsymbol{\mu}^{(k)}$. In fact, at interatomic distances of only a few hundred Bohr radii or less, even magnetic dipole-dipole coupling is negligible. We include it here because it becomes the dominant interaction beyond a distance of a thousand atomic units, as we will show in Sec. IV.

The expansion term in fourth order contributing to $H_{\rm int}$ is the electric dipole-quadrupole operator,

$$\begin{aligned} H_{\rm dq} \;=\; & -\frac{\sqrt{3}}{R^4}\left\{q^{(1)}_{1,-1}q^{(2)}_{2,+1} + \sqrt{3}q^{(1)}_{1,0}q^{(2)}_{2,0} + q^{(1)}_{1,+1}q^{(2)}_{2,-1}\right. \\ & \left. -q^{(1)}_{2,-1}q^{(2)}_{1,+1} - \sqrt{3}q^{(1)}_{2,0}q^{(2)}_{1,0} - q^{(1)}_{2,+1}q^{(2)}_{1,-1}\right\}, \end{aligned} \tag{8}$$

and finally, in $1/R^5$, we have electric quadrupole-quadrupole coupling:

$$\begin{aligned} H_{\rm qq} \;=\; & \frac{1}{R^5}\left\{q^{(1)}_{2,-2}q^{(2)}_{2,+2} + 4q^{(1)}_{2,-1}q^{(2)}_{2,+1} + 6q^{(1)}_{2,0}q^{(2)}_{2,0}\right. \\ & \left. +4q^{(1)}_{2,+1}q^{(2)}_{2,-1} + q^{(1)}_{2,+2}q^{(2)}_{2,-2}\right\}. \end{aligned} \tag{9}$$

Electric dipole-octupole interactions, which are also proportional to $1/R^5$, are neglected.

Our focus in this work is on heavy alkaline-earth atoms, in which relativistic effects are significant even in the valence shell. We will assume that the splitting between neighboring atomic energy levels corresponding to the same fine-structure manifold be larger than the interatomic interaction energy. Let both atoms be in the same well-defined

fine-structure state characterized by a total atomic angular momentum $j$ and a collective quantum number $\xi$ taking into account all other electronic degrees-of-freedom, apart from the projection quantum number $m$ of the total atomic angular momentum. Without interatomic coupling, direct products of the form

$$|j, m_1, \xi\rangle^{(1)} |j, m_2, \xi\rangle^{(2)}$$

span an energetically degenerate, $(2j+1)^2$-dimensional subspace of the full electronic Hilbert space of the diatomic system. This *uncoupled* basis of the degenerate model space formed the starting point of the approach taken by other authors [11, 20, 25]. However, in order to make most efficient use of the powerful techniques of tensor algebra and also to demonstrate and exploit inherent symmetries of the problem, we prefer to work in a *coupled* representation:

$$\begin{aligned} |J, M, \Xi\rangle \;:=\; & \sum_m C(j, j, J; m, M-m, M) \\ & \times |j, m, \xi\rangle^{(1)} |j, M-m, \xi\rangle^{(2)} . \end{aligned} \tag{10}$$

$C(j, j, J; m, M-m, M)$ is a Clebsch-Gordan coefficient [39], mediating the transformation from the uncoupled basis to the coupled one with the total electronic angular momentum $J$ running from 0 to $2j$ and $M = -J, -J+1..., J-1, J$. The capital letter $\Xi$ is employed to collectively symbolize all other electronic quantum numbers of the noninteracting diatomic system, including for example $j$.

By representing $H_{\rm int}$ in the $(2j+1)^2$-dimensional model space and diagonalizing the resulting matrix, approximate interaction energies can be obtained. Note that

$$\langle J, M, \Xi|\, H_{\rm dd} |\, J^{''}, M^{''}, \Xi\rangle = 0 \tag{11}$$

and

$$\langle J, M, \Xi|\, H_{\rm dq} |\, J^{''}, M^{''}, \Xi\rangle = 0, \tag{12}$$

because all atomic eigenstates comprising the model space have the same parity and, therefore, are not coupled by the electric dipole operator. The two atoms experience no direct electric dipole-dipole and no direct electric dipole-quadrupole interactions.

However, another important ingredient is still missing: the electric dipole-dipole dispersion interaction, which is a consequence of coupling to electronic states outside the model space. This can be included by defining complementary projection operators

$$\mathcal{P} := \sum_{J,M} |J, M, \Xi\rangle \langle J, M, \Xi| \tag{13}$$

and

$$\mathcal{Q} := \mathbf{1} - \mathcal{P}. \tag{14}$$

Let $H_0$ denote the Hamiltonian of the noninteracting system, such that

$$H_0 |J, M, \Xi\rangle = E_0(\Xi) |J, M, \Xi\rangle . \tag{15}$$

(The eigenenergies of $H_0$ depend only on atomic quantum numbers $j$ and $\xi$, not on $J$ and $M$.) According to Feshbach [40, 41], any eigenenergy $E$ of the interacting system, defined by the Schrödinger equation

$$\{H_0 + H_{\rm int}\} |\Psi\rangle = E |\Psi\rangle , \tag{16}$$

can formally be computed within the model space, provided $\mathcal{P} |\Psi\rangle \neq 0$. $\mathcal{P} |\Psi\rangle$, an element of the model space, is an eigenvector of the effective Hamiltonian

$$\begin{aligned} H_{\rm eff} \;:=\; & \mathcal{P} \{H_0 + H_{\rm int}\} \mathcal{P} \\ & + \mathcal{P} H_{\rm int} \mathcal{Q} \left[E - \mathcal{Q} \{H_0 + H_{\rm int}\} \mathcal{Q}\right]^{-1} \mathcal{Q} H_{\rm int} \mathcal{P}; \end{aligned} \tag{17}$$

the associated eigenvalue is $E$:

$$H_{\rm eff} \mathcal{P} |\Psi\rangle = E \mathcal{P} |\Psi\rangle . \tag{18}$$

By making use of Eqs. (1), (11), (12), and (15), corrections to $E_0(\Xi)$ due to interatomic coupling can be found by diagonalizing

$$H_{\rm I} := H_{\rm eff} - E_0(\Xi)\mathcal{P} = \mathcal{P}\left\{H_{\rm mm} + H_{\rm qq} + H_{\rm dis}\right\}\mathcal{P}. \tag{19}$$

$H_{\rm dis}$ is the electric dipole-dipole dispersion interaction operator, which is proportional to $1/R^6$:

$$H_{\rm dis} := H_{\rm dd}\,\mathcal{Q}\left[E_0(\Xi) - \mathcal{Q}H_0\mathcal{Q}\right]^{-1}\mathcal{Q}H_{\rm dd}. \tag{20}$$

Expansion terms of higher order in $1/R$ (as well as magnetic dipole-dipole dispersion coupling) have been dropped in Eq. (19).

### B. Coupled representation of interatomic interaction operators

Next we address the transformation properties of $H_{\rm I}$ under simultaneous rotations of atom 1 and atom 2. Since excited alkaline-earth atoms are, in general, nonspherical, it is natural to ask how the interatomic interaction reflects this lack of isotropy. To that end we seek a compact tensorial formulation of $H_{\rm mm}$, $H_{\rm qq}$, and $H_{\rm dis}$, by coupling the respective atomic tensor operators to diatomic ones. This approach also has the advantage that it enables a very systematic and elegant evaluation of matrix elements of $H_{\rm I}$ with respect to the coupled basis introduced in Eq. (10).

We first turn our attention to $H_{\rm mm}$, Eq. (6). Each direct product $\mu_m^{(1)}\mu_{-m}^{(2)}$ of atomic tensor operators can be expanded as follows:

$$\mu_m^{(1)}\mu_{-m}^{(2)} = \sum_{K=0}^{2} C(1,1,K;m,-m,0)M_{K,0}, \tag{21}$$

where

$$\begin{aligned} M_{K,0} &:= \left[\boldsymbol{\mu}^{(1)}\otimes\boldsymbol{\mu}^{(2)}\right]_{K,0} \\ &= \sum_m C(1,1,K;m,-m,0)\mu_m^{(1)}\mu_{-m}^{(2)} \end{aligned} \tag{22}$$

is the 0-component of the irreducible tensor product of rank $K$ of tensors $\boldsymbol{\mu}^{(1)}$ and $\boldsymbol{\mu}^{(2)}$. Upon inserting Eq. (21) in Eq. (6), it is easily seen that

$$H_{\rm mm} = -\frac{\sqrt{6}}{R^3}M_{2,0}, \tag{23}$$

which demonstrates the magnetic dipole-dipole interaction operator is the 0-component of a second-rank tensor. A similar argument can be applied to show that $H_{\rm qq}$ (Eq. (9)) is the 0-component of a fourth-rank tensor:

$$H_{\rm qq} = \frac{\sqrt{70}}{R^5}Q_{4,0}, \tag{24}$$

$$Q_{4,0} := \left[\boldsymbol{q}_2^{(1)}\otimes\boldsymbol{q}_2^{(2)}\right]_{4,0}. \tag{25}$$

For the purpose of uncovering the tensorial structure of the dispersion interaction operator, $H_{\rm dis}$ (Eq. (20)), we draw on considerations used by Fano and Macek in their study of the angular distribution and polarization of the light emitted by atoms excited in collision processes [42]. Greene and Zare exploited those ideas to describe the anisotropic emission of photofragments [43] and of laser-induced fluorescence [44].

In analogy to Eq. (23), the electric dipole-dipole interaction operator in Eq. (20) is

$$H_{\rm dd} = -\frac{\sqrt{6}}{R^3}D_{2,0}, \tag{26}$$

$$D_{2,0} := \left[\boldsymbol{q}_1^{(1)}\otimes\boldsymbol{q}_1^{(2)}\right]_{2,0}. \tag{27}$$

Furthermore, the operator $\mathcal{Q}\left[E_0(\Xi) - \mathcal{Q}H_0\mathcal{Q}\right]^{-1}\mathcal{Q}$ is a tensor of rank zero:

$$O_{0,0} := \mathcal{Q}\left[E_0(\Xi) - \mathcal{Q}H_0\mathcal{Q}\right]^{-1}\mathcal{Q}. \tag{28}$$

To prove this, we employ a more explicit representation of $O_{0,0}$:

$$O_{0,0} = \sum_{\Xi' \neq \Xi} \frac{1}{E_0(\Xi) - E_0(\Xi')} \times \sum_{J',M'} |J',M',\Xi'\rangle\langle J',M',\Xi'| . \tag{29}$$

Each operator $\sum_{M'} |J',M',\Xi'\rangle\langle J',M',\Xi'|$ is, according to Racah's definition of irreducible tensors [45, 46, 47], a scalar, i.e. a tensor of rank zero, since it is not difficult to see that for $m = +1, 0, -1$

$$\left[ J_m, \sum_{M'} |J',M',\Xi'\rangle\langle J',M',\Xi'| \right] = 0. \tag{30}$$

$J_{+1}$, $J_0$, and $J_{-1}$ are the spherical tensor components of the total electronic angular momentum operator $\boldsymbol{J}$. $O_{0,0}$, being a sum of scalars, is therefore also a scalar. The dispersion interaction operator can now be written as

$$\begin{aligned} H_{\rm dis} &= \frac{6}{R^6} D_{2,0} O_{0,0} D_{2,0} \\ &= \frac{6}{R^6} \sum_{K=0}^{4} C(2,2,K;0,0,0) I_{K,0} \\ &= \frac{6}{R^6} \left\{ \sqrt{\frac{1}{5}} I_{0,0} - \sqrt{\frac{2}{7}} I_{2,0} + \sqrt{\frac{18}{35}} I_{4,0} \right\}, \end{aligned} \tag{31}$$

the tensor operators $I_{K,0}$ being given by

$$I_{K,0} := \left[ [\boldsymbol{D}_2 \otimes \boldsymbol{O}_0]_2 \otimes \boldsymbol{D}_2 \right]_{K,0}, \quad K = 0, 2, 4. \tag{32}$$

In this way, a decomposition of the effective interaction operator $H_{\rm I}$ into a scalar, a second-rank tensor, and a fourth-rank tensor has been achieved:

$$\begin{aligned} H_{\rm I} &= \mathcal{P} \{ T_{0,0} + T_{2,0} + T_{4,0} \} \mathcal{P}, \\ T_{0,0} &:= \frac{6}{R^6} \sqrt{\frac{1}{5}} I_{0,0}, \\ T_{2,0} &:= -\frac{6}{R^6} \sqrt{\frac{2}{7}} I_{2,0} - \frac{\sqrt{6}}{R^3} M_{2,0}, \\ T_{4,0} &:= \frac{6}{R^6} \sqrt{\frac{18}{35}} I_{4,0} + \frac{\sqrt{70}}{R^5} Q_{4,0}. \end{aligned} \tag{33}$$

(The projection operator $\mathcal{P}$ is a scalar, in view of Eq. (30).) The physical significance of this result lies in the distinct transformation properties of the three different tensor types under rotations generated by $\boldsymbol{J}$. These are rotations of the two atoms about their respective centers. The scalar term, $T_{0,0}$, is invariant under such rotations: It describes a purely isotropic interaction. The anisotropy of the long-range interaction between two metastable alkaline-earth atoms is a consequence of the presence of the two higher-rank tensors. $T_{2,0}$ transforms like the spherical harmonic $Y_{2,0}$ (a "d-orbital"), $T_{4,0}$ like $Y_{4,0}$ (a "g-orbital"). Of course, rotations about the $z$-axis—the interatomic axis—leave all tensorial terms of $H_{\rm I}$ invariant.

### C. Reduced matrix elements

We next focus on the representation of $H_{\rm I}$ with respect to the coupled basis of the model space, Eq. (10). By putting to use the celebrated Wigner-Eckart theorem [48], the matrix elements of the operator $M_{2,0}$, for instance, can be written as

$$\langle J, M, \Xi | M_{2,0} | J'', M'', \Xi \rangle = \frac{1}{\sqrt{2J+1}} C(J'', 2, J; M'', 0, M) \langle J, \Xi \parallel M_2 \parallel J'', \Xi \rangle . \tag{34}$$

The quantity $\langle J, \Xi \parallel M_2 \parallel J^{''}, \Xi\rangle$ is referred to as a *reduced matrix element*. It is independent of projection quantum numbers and, for that reason, is not specific to the body-fixed frame in which these expressions have been evaluated.

Using the definitions

$$[A, B, ..., Z] := (2A+1)(2B+1)...(2Z+1) \tag{35}$$

and

$$\langle j, \xi \parallel \mu^{(1)} \parallel j, \xi\rangle = \langle j, \xi \parallel \mu^{(2)} \parallel j, \xi\rangle =: \langle j, \xi \parallel \mu \parallel j, \xi\rangle\,, \tag{36}$$

standard Wigner-Racah algebra allows a straightforward evaluation of the reduced matrix elements of the tensor $\boldsymbol{M}_2$:

$$\langle (jj)J, \Xi \parallel \left[\boldsymbol{\mu}^{(1)} \otimes \boldsymbol{\mu}^{(2)}\right]_2 \parallel (jj)J^{''}, \Xi\rangle = [J, 2, J^{''}]^{1/2} \left\{ \begin{array}{ccc} j & j & 1 \\ j & j & 1 \\ J & J^{''} & 2 \end{array} \right\} \langle j, \xi \parallel \mu \parallel j, \xi\rangle^2\,. \tag{37}$$

The 9-j symbol [49] in this expression satisfies the equation

$$\left\{ \begin{array}{ccc} j & j & 1 \\ j & j & 1 \\ J & J^{''} & 2 \end{array} \right\} = (-1)^{J+J^{''}} \left\{ \begin{array}{ccc} j & j & 1 \\ j & j & 1 \\ J & J^{''} & 2 \end{array} \right\}. \tag{38}$$

This is a simple consequence of the symmetry properties of 9-j symbols under interchange of two of its rows and the fact that both atoms have, within the model space, the same angular momentum, $j$. (The two atoms would not have to be of the same species, however.) Hence, $\langle J, \Xi \parallel M_2 \parallel J^{''}, \Xi\rangle = 0$, if $J + J^{''}$ is odd. In other words, states of even and odd $J$ are not coupled by $\boldsymbol{M}_2$. We will show below that this is true for all operators defining $H_{\rm I}$ (Eq. (33)).

The reduced matrix element $\langle j, \xi \parallel \mu \parallel j, \xi\rangle$ in Eq. (37) can be related to the atomic magnetic dipole moment,

$$\begin{aligned} \langle \mu\rangle &:= \langle j, j, \xi | \mu_0 | j, j, \xi\rangle \\ &= \sqrt{\frac{j}{(j+1)(2j+1)}}\, \langle j, \xi \parallel \mu \parallel j, \xi\rangle\,, \end{aligned} \tag{39}$$

so that

$$\langle J, \Xi \parallel M_2 \parallel J^{''}, \Xi\rangle = \sqrt{5}[J, J^{''}]^{1/2} \left\{ \begin{array}{ccc} j & j & 1 \\ j & j & 1 \\ J & J^{''} & 2 \end{array} \right\} \frac{(j+1)(2j+1)}{j} \langle \mu\rangle^2\,. \tag{40}$$

Equation (40) is valid only if $j$ is different from zero. Otherwise, the reduced matrix element vanishes, because in this case the first and second row of the 9-j symbol in Eq. (37) do not satisfy the triangle condition and the 9-j symbol therefore vanishes.

Finding the reduced matrix elements of $\boldsymbol{Q}_4$ is equally easy. We introduce the atomic quadrupole moment as

$$\begin{aligned} \langle q_2\rangle &:= 2\,\langle j, j, \xi | q_{2,0} | j, j, \xi\rangle \\ &= 2\sqrt{\frac{j(2j-1)}{(j+1)(2j+1)(2j+3)}}\, \langle j, \xi \parallel q_2 \parallel j, \xi\rangle \end{aligned} \tag{41}$$

and obtain for $j \geq 1$

$$\langle J, \Xi \parallel Q_4 \parallel J^{''}, \Xi\rangle = \frac{3}{4}[J, J^{''}]^{1/2} \left\{ \begin{array}{ccc} j & j & 2 \\ j & j & 2 \\ J & J^{''} & 4 \end{array} \right\} \frac{(j+1)(2j+1)(2j+3)}{j(2j-1)} \langle q_2\rangle^2\,. \tag{42}$$

Because of properties of the 9-j symbol, the reduced matrix element $\langle J, \Xi \parallel Q_4 \parallel J^{''}, \Xi\rangle$ vanishes if $j = 0$ or $1/2$ or if $(-1)^{J+J^{''}}$ is negative.

Evaluating the reduced matrix elements of the dispersion interaction tensors $\boldsymbol{I}_K$ ($K = 0, 2, 4$) is slightly more involved. We apply the well-known rules for determining reduced matrix elements of an irreducible tensor product of noncommuting tensor operators and arrive at

$$\begin{aligned}\langle J,\Xi \parallel I_K \parallel J^{''},\Xi\rangle \;=\; (-1)^{J+J^{''}}\sqrt{2K+1}\sum_{\Xi'\neq\Xi}\sum_{J'}\left\{\begin{array}{ccc} 2 & 2 & K \\ J^{''} & J & J^{'}\end{array}\right\} \\ \times\frac{\langle J,\Xi \parallel D_2 \parallel J^{'},\Xi^{'}\rangle\langle J^{'},\Xi^{'} \parallel D_2 \parallel J^{''},\Xi\rangle}{E_0(\Xi)-E_0(\Xi^{'})}.\end{aligned} \tag{43}$$

The coupling by the interaction tensor of rank $K$ between the two electronic states of angular momentum $J$ and $J^{''}$, respectively, is controlled by the 6-j symbol [49] in Eq. (43). In particular, $K$, $J$, and $J^{''}$ must satisfy the triangle condition $|J-K| \leq J^{''} \leq J+K$. The reduced matrix elements of $\boldsymbol{D}_2$ require a treatment similar to the one that led to Eq. (37). Before writing down the final result for $\langle J,\Xi \parallel I_K \parallel J^{''},\Xi\rangle$, however, we need to discuss the notation we will employ.

Let $\varepsilon(j^{(k)},\xi^{(k)},j,\xi)$ denote the transition energy associated with the transition of atom $k$ from the state $\mid j,\xi\rangle$ to $\mid j^{(k)},\xi^{(k)}\rangle$, and $f(j^{(k)},\xi^{(k)},j,\xi)$ be the corresponding dipole oscillator strength [50]:

$$\begin{aligned}f(j^{(k)},\xi^{(k)},j,\xi) \;:=\; \frac{2}{3}\frac{(-1)^{j-j^{(k)}}}{2j+1}\varepsilon(j^{(k)},\xi^{(k)},j,\xi) \\ \times\langle j,\xi \parallel q_1 \parallel j^{(k)},\xi^{(k)}\rangle\langle j^{(k)},\xi^{(k)} \parallel q_1 \parallel j,\xi\rangle.\end{aligned} \tag{44}$$

We use these to define an intermediate dispersion coefficient

$$\begin{aligned}B(j^{(1)},j^{(2)},j,\xi) \;:=\; (-1)^{1+j^{(1)}-j^{(2)}} \\ \times{\sum_{\xi^{(1)}}}^{'}{\sum_{\xi^{(2)}}}^{'}\frac{f(j^{(1)},\xi^{(1)},j,\xi)f(j^{(2)},\xi^{(2)},j,\xi)}{\left\{\varepsilon(j^{(1)},\xi^{(1)},j,\xi)+\varepsilon(j^{(2)},\xi^{(2)},j,\xi)\right\}\varepsilon(j^{(1)},\xi^{(1)},j,\xi)\varepsilon(j^{(2)},\xi^{(2)},j,\xi)}.\end{aligned} \tag{45}$$

$\sum_{\xi^{(k)}}^{'}$ indicates a sum over all atomic eigenstates with angular momentum $j^{(k)}$, excluding $\xi^{(k)}=\xi$ if $j^{(k)}=j$. The relation between our $B$-coefficients and the intermediate $C_6$-coefficients used by Derevianko *et al.* [25] is

$$C_6^{j^{(1)}j^{(2)}} = -\frac{27}{8}(2j+1)^2 B(j^{(1)},j^{(2)},j,\xi). \tag{46}$$

On physical grounds we expect only those $j^{(k)}$ to play a role that are consistent with dipole-allowed transitions. This fact is expressed by the triangle conditions that must be satisfied in the function

$$A(J,J^{''},K,j,j^{(1)},j^{(2)}) := \sum_{J'}(2J^{'}+1)\left\{\begin{array}{ccc} 2 & 2 & K \\ J^{''} & J & J^{'}\end{array}\right\}\left\{\begin{array}{ccc} j & j^{(1)} & 1 \\ j & j^{(2)} & 1 \\ J & J^{'} & 2\end{array}\right\}\left\{\begin{array}{ccc} j^{(1)} & j & 1 \\ j^{(2)} & j & 1 \\ J^{'} & J^{''} & 2\end{array}\right\}. \tag{47}$$

Specifically, $j$, $j^{(k)}$, and 1 must form a triangle for $A$ not to vanish.

Using definitions (45) and (47), the reduced matrix elements of $\boldsymbol{I}_K$ assume a rather compact form:

$$\begin{aligned}\langle J,\Xi \parallel I_K \parallel J^{''},\Xi\rangle \;=\; \frac{45}{4}(2j+1)^2[J,K,J^{''}]^{1/2} \\ \times\sum_{j^{(1)}}\sum_{j^{(2)}}A(J,J^{''},K,j,j^{(1)},j^{(2)})B(j^{(1)},j^{(2)},j,\xi).\end{aligned} \tag{48}$$

It is interesting to see why $\langle J,\Xi \parallel I_K \parallel J^{''},\Xi\rangle$ vanishes if $J+J^{''}$ is odd. First note that $B(j^{(1)},j^{(2)},j,\xi)$ is symmetric under interchange of $j^{(1)}$ and $j^{(2)}$, since $\xi^{(1)}$ and $\xi^{(2)}$ are just dummy summation variables, which may be renamed. (This statement relies on the premise that both atoms are identical and described by the same unperturbed quantum state $\mid j,\xi\rangle$.) An immediate consequence of this observation and the dipole-selection rules is the number of independent B-coefficients: For $j \geq 1$ there are six, corresponding to the combinations $\{j^{(1)}=j+1, j^{(2)}=j+1\}$, $\{j^{(1)}=j+1, j^{(2)}=j\}$, $\{j^{(1)}=j+1, j^{(2)}=j-1\}$, $\{j^{(1)}=j, j^{(2)}=j\}$, $\{j^{(1)}=j, j^{(2)}=j-1\}$, and $\{j^{(1)}=j-1, j^{(2)}=j-1\}$. Second, by exploiting the symmetry properties of the 9-j symbols in Eq. (47), it can be shown that

$$A(J,J^{''},K,j,j^{(2)},j^{(1)}) = (-1)^{J+J^{''}}A(J,J^{''},K,j,j^{(1)},j^{(2)}). \tag{49}$$

Hence,

$$\begin{aligned} & \sum_{j^{(1)}} \sum_{j^{(2)}} A(J, J^{''}, K, j, j^{(1)}, j^{(2)}) B(j^{(1)}, j^{(2)}, j, \xi) \\ = & \sum_{j^{(2)}} \sum_{j^{(1)}} A(J, J^{''}, K, j, j^{(2)}, j^{(1)}) B(j^{(2)}, j^{(1)}, j, \xi) \\ = & (-1)^{J+J^{''}} \sum_{j^{(1)}} \sum_{j^{(2)}} A(J, J^{''}, K, j, j^{(1)}, j^{(2)}) B(j^{(1)}, j^{(2)}, j, \xi). \end{aligned} \tag{50}$$

$\sum_{j^{(1)}} \sum_{j^{(2)}} A(J, J^{''}, K, j, j^{(1)}, j^{(2)}) B(j^{(1)}, j^{(2)}, j, \xi)$ in Eq. (48) is therefore identical to zero if $J + J^{''}$ is odd.

## III. MOLECULAR ROTATIONS IN EXTERNAL MAGNETIC FIELD

### A. Invariant formulation of interatomic interaction Hamiltonian

Suppose each of the two atoms were in a spherically symmetric electronic state ($j = 0$, $m = 0$), defined with respect to a quantization axis held fixed in the laboratory frame. In this case, the interatomic interaction energy clearly does not depend on the orientation of the diatomic axis relative to the quantization axis. If, however, the atoms are nonspherical ($j > 0$), then the anisotropic forces, as expressed through the tensorial structure of the effective interaction operator $H_{\rm I}$ in Eq. (33), attempt to align the atomic angular momenta along the diatomic axis. The relative orientation of diatomic axis and laboratory-fixed quantization axis now matters. This leads to a coupling between electronic degrees-of-freedom and molecular rotations. In order to put this intuitive picture into more quantitative terms, we need a formulation of $H_{\rm I}$ that makes use only of observables specific to the laboratory frame.

Let $U$ be a rotation operator from the laboratory $z$-axis to the body-fixed $z$-axis. This operator connects each tensor $T_{K,0}$ in Eq. (33) with the 0-component of the tensor $\boldsymbol{T}_K$ measured in the laboratory frame:

$$T_{K,0}^{(\rm Lab)} := U^{-1} T_{K,0} U. \tag{51}$$

On the other hand, the operator $U T_{K,0}^{(\rm Lab)} U^{-1}$ is just a linear combination of tensor components $T_{K,M}^{(\rm Lab)}$, $M = -K, ..., +K$. The expansion coefficients are the elements of the appropriate rotation matrix:

$$T_{K,0} = \sum_M \mathcal{D}_{M,0}^{(K)}(\varphi, \vartheta, 0) T_{K,M}^{(\rm Lab)}. \tag{52}$$

Here, $\vartheta$ and $\varphi$ are the polar and the azimuthal angle, respectively, of the diatomic axis in the laboratory frame. Since for integer $K$

$$\mathcal{D}_{M,0}^{(K)}(\varphi, \vartheta, 0) = (-1)^M C_{K,-M}(\vartheta, \varphi) \tag{53}$$

(see, for example, Ref. [39]), the expansion coefficients in Eq. (52) can also be interpreted as the components of a spherical tensor of rank $K$, defined with respect to rotations generated by $\boldsymbol{L}$, the angular momentum operator of the diatomic axis. Thus,

$$T_{K,0} = \sqrt{2K+1}\, [\boldsymbol{C}_K \otimes \boldsymbol{T}_K]_{0,0}\,, \tag{54}$$

which demonstrates $T_{K,0}$ is a tensor of rank zero with respect to rotations generated by the total angular momentum $\boldsymbol{J}_{\rm tot} = \boldsymbol{L} + \boldsymbol{J}$. Under rotations of all particles—electrons and nuclei—$H_{\rm I}$ is therefore totally invariant:

$$H_{\rm I} = \sum_{K=0,2,4} \sqrt{2K+1}\, [\boldsymbol{C}_K \otimes \mathcal{P}\boldsymbol{T}_K \mathcal{P}]_{0,0}\,. \tag{55}$$

Let $|L, M_L\rangle$ denote an eigenstate of $\boldsymbol{L}^2$ and $L_z$. Eigenstates of $\boldsymbol{J}_{\rm tot}^2$ and $J_{{\rm tot},z}$ are then generated by coupling nuclear and electronic angular momentum states as usual:

$$\begin{aligned} |J_{\rm tot}, M_{\rm tot}, L, J\rangle \;:=\; & \sum_{M_L} C(L, J, J_{\rm tot}; M_L, M_{\rm tot} - M_L, M_{\rm tot}) \\ & \times |L, M_L\rangle\, |J, M_{\rm tot} - M_L, \Xi\rangle\,. \end{aligned} \tag{56}$$

We next determine the representation of $H_{\rm I}$ in this basis. Application of the Wigner-Eckart theorem gives

$$\langle J_{\rm tot}, M_{\rm tot}, L, J|\, H_{\rm I}\,|\, J_{\rm tot}^{''}, M_{\rm tot}^{''}, L^{''}, J^{''}\,\rangle = \frac{\delta_{J_{\rm tot},J_{\rm tot}^{''}}\,\delta_{M_{\rm tot},M_{\rm tot}^{''}}}{\sqrt{2J_{\rm tot}+1}}\,\langle J_{\rm tot}, L, J\parallel H_{\rm I}\parallel J_{\rm tot}, L^{''}, J^{''}\,\rangle\,. \tag{57}$$

Of course, for the scalar tensor $H_{\rm I}$, $J_{\rm tot}$ and $M_{\rm tot}$ are good quantum numbers.

$L$ and $J$, however, are typically not conserved. This is most easily seen by inspection of the reduced matrix element in Eq. (57):

$$\begin{aligned}\langle J_{\rm tot}, L, J\parallel H_{\rm I}\parallel J_{\rm tot}, L^{''}, J^{''}\,\rangle \;=\; & (-1)^{J_{\rm tot}+J+L^{''}}\sqrt{2J_{\rm tot}+1} \\ & \times\sum_{K=0,2,4}\left\{\begin{array}{ccc} L & L^{''} & K \\ J^{''} & J & J_{\rm tot}\end{array}\right\} \\ & \times\langle L\parallel C_K\parallel L^{''}\,\rangle\,\langle J,\Xi\parallel T_K\parallel J^{''},\Xi\rangle\,.\end{aligned} \tag{58}$$

The reduced matrix element of $\boldsymbol{C}_K$ is that of a renormalized spherical harmonic (cf. Eq. (4)) and is well known [49]:

$$\langle L\parallel C_K\parallel L^{''}\,\rangle = \sqrt{2L''+1}C(L^{''},K,L;0,0,0). \tag{59}$$

Hence, it vanishes if $L+L^{''}$ is odd. Otherwise, for $K=2$ and 4, there can be coupling between rotational states of different quantum numbers $L$ and $L^{''}$, provided $L$, $L^{''}$, and $K$ form a triangle. This coupling exists only if the atomic angular momentum $j$ is larger than zero, because only then do $\langle J,\Xi\parallel T_2\parallel J^{''},\Xi\rangle$ ($j\geq 1/2$) and $\langle J,\Xi\parallel T_4\parallel J^{''},\Xi\rangle$ ($j\geq 1$) in general not vanish. The reduced matrix elements of $\boldsymbol{T}_K$ for $K=0,2,4$ follow immediately by combining Eqs. (33), (40), (42), and (48), and from our analysis in Sec.II C we already know that $H_{\rm I}$ conserves $(-1)^J$, but not the total electronic angular momentum $J$ itself.

### B. Zeeman operator and rotation energy

Precise experimental studies of long-range interactions can be carried out with cold, magnetic atoms trapped by means of suitable magnetic field configurations [51]. The presence of an externally applied magnetic field $\boldsymbol{B}$ breaks the local rotational invariance, and $J_{\rm tot}$ is no longer expected to be a good quantum number. To model this situation, we make the simplifying assumption that $\boldsymbol{B}$ is homogeneous: $\boldsymbol{B}=\mathcal{B}\boldsymbol{e}_z$. The complete Hamiltonian describing the relative motion of two interacting atoms, with reduced mass $m_{\rm red}$, exposed to a magnetic field is thus

$$H = -\frac{1}{2m_{\rm red}}\left\{\frac{\partial^2}{\partial R^2}+\frac{2}{R}\frac{\partial}{\partial R}\right\}+\frac{\boldsymbol{L}^2}{2m_{\rm red}R^2}+H_{\rm I}-(\boldsymbol{\mu}^{(1)}+\boldsymbol{\mu}^{(2)})_0\mathcal{B}. \tag{60}$$

The internal energy, $E_0(\Xi)$, of the two atoms (see Eq. (15)) has been set to zero.

By representing $H$ in the coupled basis defined in Eq. (56), a natural diabatic representation is obtained that can be used for rigorous scattering calculations. Alternatively, the sum of the matrices of the rotational kinetic energy operator, $\frac{\boldsymbol{L}^2}{2m_{\rm red}R^2}$, the interatomic interaction operator, $H_{\rm I}$, and the Zeeman operator, $-(\boldsymbol{\mu}^{(1)}+\boldsymbol{\mu}^{(2)})_0\mathcal{B}$ can be diagonalized as a function of $R$. This approach yields adiabatic potential energy curves. The dynamics on these curves is driven by the radial kinetic energy operator, $-\frac{1}{2m_{\rm red}}\left\{\frac{\partial^2}{\partial R^2}+\frac{2}{R}\frac{\partial}{\partial R}\right\}$.

The calculation of the matrix elements of $\frac{\boldsymbol{L}^2}{2m_{\rm red}R^2}$ is a trivial matter,

$$\langle J_{\rm tot}, M_{\rm tot}, L, J|\,\frac{\boldsymbol{L}^2}{2m_{\rm red}R^2}\,|\, J_{\rm tot}^{''}, M_{\rm tot}^{''}, L^{''}, J^{''}\,\rangle = \frac{L(L+1)}{2m_{\rm red}R^2}\delta_{J_{\rm tot},J_{\rm tot}^{''}}\,\delta_{M_{\rm tot},M_{\rm tot}^{''}}\,\delta_{L,L''}\delta_{J,J''}\,, \tag{61}$$

and the treatment of $H_{\rm I}$ was the subject of the previous subsection. The Zeeman operator is discussed in the following. Again, we utilize Wigner-Racah algebra by noting that $-(\boldsymbol{\mu}^{(1)}+\boldsymbol{\mu}^{(2)})_0\mathcal{B}$ is the 0-component of a rank-one tensor. It is independent of the orientation of the diatomic axis and therefore does not couple rotational states of different $L$.

Interestingly, at least in the case of identical atoms, it also does not couple electronic states of different $J$. To understand this, consider the electronic reduced matrix elements of $\boldsymbol{\mu}^{(1)}+\boldsymbol{\mu}^{(2)}$ ($j>0$):

$$\begin{aligned}\langle J,\Xi\parallel \mu^{(1)}+\mu^{(2)}\parallel J^{''},\Xi\rangle \;=\; & (-1)^{J+2j+1}\left((-1)^{J+J^{''}}+1\right)[J,J^{''}]^{1/2} \\ & \times\left\{\begin{array}{ccc} j & j & 1 \\ J^{''} & J & j\end{array}\right\}\sqrt{\frac{(j+1)(2j+1)}{j}}\,\langle\mu\rangle\,.\end{aligned} \tag{62}$$

TABLE I: Parameters needed for a quantitative characterization of the long-range interaction between two metastable (5s5p) $^3P_2$ strontium atoms. $\langle\mu\rangle$ (Eq. (39)) is the magnetic dipole moment, $\langle q_2\rangle$ (Eq. (41)) the electric quadrupole moment, and the coefficients $B_{j^{(1)},j^{(2)}}$ (Eq. (45)) are needed to describe electric dipole-dipole dispersion coupling. The subscripts indicate that in the dispersion interaction process one atom makes a virtual dipole transition from $j = 2$ to $j^{(1)}$ and the other one from $j = 2$ to $j^{(2)}$. The parameters obtained in this work were calculated within a semiempirical approach. Derevianko *et al.* [25] presented *ab initio* results; their intermediate dispersion coefficients have been converted using Eq. (46). The one-standard deviation uncertainties cited in Ref. [25] are given in parentheses. All data are in atomic units.

| | This work | Ref. [25] |
|---|---|---|
| $\langle\mu\rangle$ | -3.00 | |
| $\langle q_2\rangle$ | 15.4 | 15.6(5) |
| $B_{1,1}$ | -132 | -158(16) |
| $B_{2,1}$ | 187 | 203(20) |
| $B_{2,2}$ | -266 | -264(26) |
| $B_{3,1}$ | -343 | -415(42) |
| $B_{3,2}$ | 497 | 555(56) |
| $B_{3,3}$ | -1020 | -1290(130) |

Owing to the factor $(-1)^{J+J''}+1$, the reduced matrix element vanishes if $J+J''$ is odd. In addition, however, the 6-j symbol in Eq. (62) differs from zero only if $|J-1| \le J'' \le J+1$. Since, for atoms of the same species, $J$ and $J''$ are integers, it can be concluded that $J$ must equal $J''$. The physical origin of this selection rule is the tensorial rank of the magnetic dipole operator.

Using this result, it is now straightforward to write down the matrix elements of the Zeeman operator:

$$\langle J_{\rm tot}, M_{\rm tot}, L, J| - (\boldsymbol{\mu}^{(1)}+\boldsymbol{\mu}^{(2)})_0\mathcal{B}\,|\, J''_{\rm tot}, M''_{\rm tot}, L'', J''\,\rangle = (-1)^{J_{\rm tot}+L+J}\delta_{M_{\rm tot},M''_{\rm tot}}\,\delta_{L,L''}\delta_{J,J''} \tag{63}$$
$$\times C(J''_{\rm tot},1,J_{\rm tot};M_{\rm tot},0,M_{\rm tot})\sqrt{2J''_{\rm tot}+1}\left\{\begin{array}{ccc} J & J & 1\\ J''_{\rm tot} & J_{\rm tot} & L\end{array}\right\}\langle J,\Xi\parallel \mu^{(1)}+\mu^{(2)}\parallel J,\Xi\rangle\,\mathcal{B}.$$

Thus we have shown that the matrix representation of the Zeeman operator is diagonal in all angular momentum quantum numbers except $J_{\rm tot}$. The Clebsch-Gordan coefficient (as well as the 6-j symbol) in Eq. (63) imposes a restriction on the total angular momentum quantum numbers that can be coupled: $J_{\rm tot}$ and $J''_{\rm tot}$ may not differ by more than one unit.

## IV. APPLICATION TO METASTABLE STRONTIUM

### A. Atomic parameters

In this section we present an application of the theory developed in Secs. II and III to collisions between cold, metastable $^{88}$Sr atoms. The mass of $^{88}$Sr [52] is $1.60280\times10^5$ a.u. The other atom-specific parameters needed are the magnetic dipole moment, $\langle\mu\rangle$ (Eq. (39)), the electric quadrupole moment, $\langle q_2\rangle$ (Eq. (41)), and the intermediate dispersion coefficients $B(j^{(1)},j^{(2)},j,\xi) =: B_{j^{(1)},j^{(2)}}$ (Eq. (45)). Here, $j = 2$, and $\xi$ is specified in terms of the other quantum numbers characterizing the (5s5p) $^3P_2$ state of atomic strontium. We have performed semiempirical electronic-structure calculations to determine $\langle\mu\rangle$, $\langle q_2\rangle$, and $B_{j^{(1)},j^{(2)}}$.

Atomic strontium can be regarded as a two-electron system, at least on the excitation energy scale of just a few electron volts relevant to the present study. This realization can be exploited to efficiently compute and successfully reproduce the amazing complexity of photoabsorption Rydberg spectra of alkaline-earth atoms. A detailed and general description of the underlying concepts, formal developments, and applications is given in Ref. [53].

In a first step, we concentrate on the one-electron physics of $Sr^+$. The single valence electron moves in the field of a closed-shell ionic core. The effective, spherically symmetric potential the electron experiences is assumed to be of the form

$$\mathcal{V}_l(r) = -\frac{1}{r}\left\{2+(Z-2)\exp\left(-\alpha_{l,1}r\right)+\alpha_{l,2}r\exp\left(-\alpha_{l,3}r\right)\right\}-\frac{\alpha_{\rm cp}}{2r^4}\left\{1-\exp\left[-(r/r_l)^6\right]\right\}. \tag{64}$$

TABLE II: Order-of-magnitude estimates of the energies, in atomic units, associated with magnetic dipole-dipole coupling ($E_{\rm mm}$), electric quadrupole-quadrupole coupling ($E_{\rm qq}$), electric dipole-dipole dispersion interaction ($E_{\rm dis}$), and molecular rotation ($E_{\rm rot}$) of two metastable strontium atoms separated by a distance of $R$ Bohr radii.

| $R$ | $E_{\rm mm}$ | $E_{\rm qq}$ | $E_{\rm dis}$ | $E_{\rm rot}$ |
|---|---|---|---|---|
| 10 | $10^{-7}$ | $10^{-3}$ | $10^{-3}$ | $10^{-7}$ |
| $10^2$ | $10^{-10}$ | $10^{-8}$ | $10^{-9}$ | $10^{-9}$ |
| $10^3$ | $10^{-13}$ | $10^{-13}$ | $10^{-15}$ | $10^{-11}$ |
| $10^4$ | $10^{-16}$ | $10^{-18}$ | $10^{-21}$ | $10^{-13}$ |

This one-electron potential is physically well motivated: At large distances from the ionic core, the electron feels the attraction by a practically pointlike $Sr^{++}$ ion. As the electron comes closer, the ionic core responds to the presence of the electron and becomes polarized. $\alpha_{\rm cp} = 7.5$ a.u. is the dipole polarizability of $Sr^{++}$ [54]. Below the empirical cutoff radius $r_l$, there is a transition, mediated by the term proportional to $\alpha_{l,2}$, from the exterior to the interior region of the ionic core. The electron interacts with an unscreened nucleus of charge $Z = 38$ at $r$ much smaller than $1/\alpha_{l,1}$. Note that the parameters $\alpha_{l,i}$ and $r_l$ are assumed to be dependent on the orbital angular momentum quantum number $l$ of the valence electron. They are determined by comparing the theoretical excitation spetrum computed on the basis of Eq. (64) with experimental data on $Sr^+$; the values used in this work were taken from Ref. [53].

Another important interaction operator must be included for a quantitative description of heavy alkaline-earth atoms: spin-orbit interaction, which we use in the form [55]

$$\mathcal{V}_l^{(\rm so)} = \frac{\boldsymbol{s}\cdot\boldsymbol{l}}{2c^2}\frac{1}{r}\frac{{\rm d}\mathcal{V}_l}{{\rm d}r}\left[1-\frac{\mathcal{V}_l}{2c^2}\right]^{-2}. \tag{65}$$

The factor in brackets counteracts the $r^{-3}$-divergence of $r^{-1}{\rm d}\mathcal{V}_l/{\rm d}r$ near the nucleus. $\boldsymbol{s}$ in Eq. (65) is the spin of the valence electron, and $c$ is the speed of light. $\mathcal{V}_l^{(\rm so)}$ was adapted by Ref. [56] into the framework of eigenchannel R-matrix calculations and utilized to compute precise photodetachment spectra of the heavy alkali-metal anions.

The quantum-mechanical motion of an electron exposed to the potential $\mathcal{V}_l + \mathcal{V}_l^{(\rm so)}$ is solved using a finite-element basis [57, 58, 59] for the radial degree-of-freedom. A radial box size of 25 Bohr radii and 600 finite-element functions, corresponding to a quadratically spaced grid of 200 sectors inside the box and three functions in each sector, have proved to be sufficient. The $Sr^+$ model Hamiltonian $h$, which comprises kinetic energy and effective potential, is represented and diagonalized in a product basis of finite-element and spin-angular [48] functions up to $l = 6$ (i-orbitals). For each combination of orbital and total angular momentum quantum numbers of the single valence electron, the 18 energetically lowest radial eigenfunctions—excluding of course the filled inner-shell states—are selected. A two-electron basis set is then constructed by coupling pairs of the selected eigenstates of the one-electron Hamiltonian $h$, performing the angular momentum algebra within the $jj$-coupling scheme. Denoting the electron-electron Coulomb repulsion as $1/r_{12}$, the eigenenergies and eigenstates of the valence shell of atomic strontium are obtained by diagonalizing the matrix representation of $h(1) + h(2) + 1/r_{12}$ in the two-electron basis set. In this way the complicated dynamics of the two correlated valence electrons is treated to a high degree of accuracy.

The direct numerical evaluation of Eqs. (39), (41), and (45) using the two-electron eigenvectors is straightforward. Our results for the atomic parameters, which are converged with respect to all basis set parameters described above, are shown in Table I, together with the *ab initio* data presented by Derevianko *et al.* [25]. The magnetic dipole moment of metastable $^{88}$Sr was not explicitly discussed in Ref. [25]. In a $^3P_2$ state it seems natural to assume an atomic spin of 1, consistent with a magnetic dipole moment of $-3$. However, due to spin-orbit interaction the total spin is not really a good quantum number, and it had to be checked that the degree of spin symmetry violation is negligible. This is, in fact, the case. Our calculated electric quadrupole moment agrees well with that of Ref. [25]; the intermediate dispersion coefficients also agree, to within the 10% one-standard deviation uncertainty of the data quoted by Derevianko and co-workers [25].

### B. Diatomic potential energy curves and scattering lengths

Before we turn our attention to quantitative results on the interaction energies between metastable Sr atoms, it is helpful to explore the relative importance of the different interaction operators we have analyzed in Secs. II and III. To that end we have collected in Table II simple order-of-magnitude estimates as a function of interatomic separation. They are easily obtained by using the parameters in Table I and diagonalizing the individual terms the interatomic interaction operator, $H_{\rm I}$ (Eq. (33)), consists of, represented in the coupled basis of the electronic model space, Eq. (10).

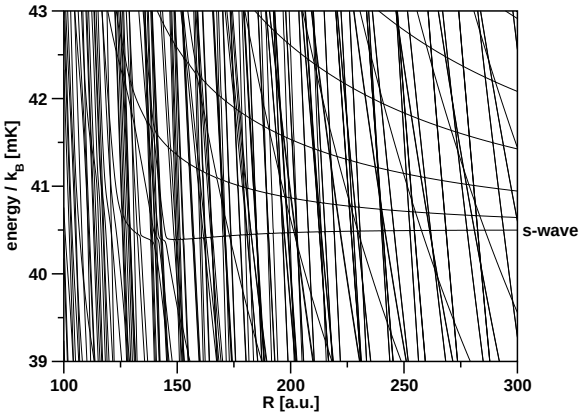


FIG. 1: Adiabatic potential energy curves of two metastable strontium atoms ((5s5p) $^3P_2$) in a magnetic field of 100 G, obtained by diagonalizing the matrix $\boldsymbol{V}$ defined in Eq. (66). The total angular momentum projection quantum number, $M_{\rm tot}$, is +4. The marked curve correlates at large interatomic separations to two fully polarized strontium atoms (atomic projection quantum number $m = +2$) in a rotational s-wave state ($L = 0$). A basis describing molecular rotations in the laboratory frame with elements up to $L = 40$ has been employed in the calculation.

Table II allows us to draw several important conclusions. Between distances of 100 and 1000 Bohr radii the electric quadrupole-quadrupole interaction dominates. Only as $R = 10$ is approached, the electric dipole-dipole dispersion interaction becomes comparable. However, at these relatively small distances the interaction energies are comparable with the fine-structure splitting between the (5s5p) $^3P_2$ and the (5s5p) $^3P_1$ state, which is of order $10^{-3}$ Hartree. In other words, at distances much lower than 100 Bohr radii the electronic model space we have chosen in Sec. II is no longer appropriate. Truncating all interaction operators of orders higher than six in $1/R$ (Eq. (19)) also becomes highly questionable under these circumstances. At $R \geq 100$ a.u., however, the formalism developed in this paper may be expected to be useful for quantitative predictions.

In the long-range limit, at $R$ larger than 1000 Bohr radii, magnetic dipole-dipole coupling remains the only relevant interatomic interaction mechanism. Also shown in Table II are the characteristic energy quanta associated with the rotational motion of the diatomic system. They are comparable with dispersion energies around distances of $R = 100$, but become dominant at interatomic separations of 1000 Bohr radii and more. As is well known, at ultracold temperatures only rotational s-waves remain unaffected by the long-range rotational barrier and can probe interatomic interaction properties. In the presence of an external magnetic field, another energy scale must be taken into consideration: the Zeeman splitting, which is of order $10^{-7}$ Hartree for a magnetic field strength of 100 Gauss. Hence, typical laboratory fields are unable to distort the spin-orbit coupling pattern in $^{88}$Sr, and our assumption of uncoupled fine-structure states remains valid.

Figures 1, 2, and 3 display adiabatic potential energy curves of two metastable strontium atoms exposed to a magnetic field of 100 G. The curves were calculated by diagonalizing, as a function of $R$, the matrix

$$\begin{aligned} \langle J_{\rm tot}, M_{\rm tot}, L, J| \, \frac{\boldsymbol{L}^2}{2m_{\rm red}R^2} + H_{\rm I} - (\boldsymbol{\mu}^{(1)} + \boldsymbol{\mu}^{(2)})_0 \mathcal{B} \, | \, J_{\rm tot}^{''}, M_{\rm tot}^{''}, L^{''}, J^{''} \, \rangle \\ =: \langle J_{\rm tot}, M_{\rm tot}, L, J| \, V \, | \, J_{\rm tot}^{''}, M_{\rm tot}^{''}, L^{''}, J^{''} \, \rangle \, , \end{aligned} \tag{66}$$

i.e., the sum of the matrices of the rotational kinetic energy operator (Eq. (61)), the interatomic interaction operator (Eqs. (57) and (58)), and the Zeeman operator (Eq. (63)). Exploiting the symmetry properties of $V$, we selected a basis characterized by even rotational and even electronic angular momentum quantum numbers. In our numerical studies we included rotational quantum numbers up to $L_{\rm max} = 40$, which gave converged results.

Of immediate interest for magnetic trap experiments are low-field seeking atomic states. For $j = 2$ these are the ones with projection quantum numbers $m = +1$ and $+2$. If both atoms are fully polarized ($m = +2$) and in a rotational s-wave state (this is associated with a molecular eigenstate only at large interatomic separations), then the total angular momentum projection quantum number, $M_{\rm tot}$, is +4. $M_{\rm tot}$ is conserved at all stages of a collision between the two atoms. The energetically highest Zeeman manifold with $M_{\rm tot} = +4$ is depicted in Fig. 1. The potential energy curve correlating to the rotational s-wave is indicated in the figure. The behavior of the s-wave energy differs significantly from that of the curves deriving from higher rotational states, which are clearly repulsive. The s-wave curve is attractive at distances larger than 150 Bohr radii and becomes repulsive at smaller radii. Near the minimum of the resulting potential well there are several avoided crossings, which lead to inelastic losses through

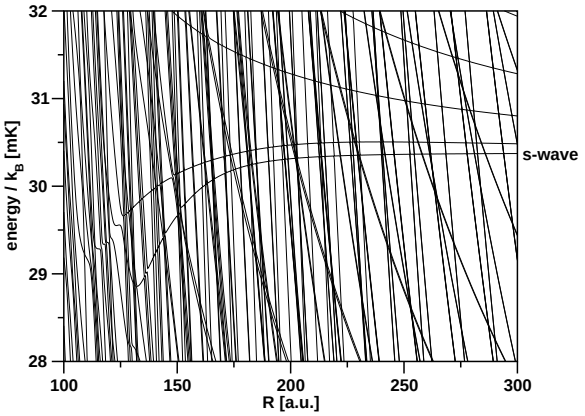


FIG. 2: Adiabatic potential energy curves of two metastable strontium atoms ((5s5p) $^3P_2$) in a magnetic field of 100 G. In this case $M_{\rm tot} = +3$. The energy region shown corresponds to the Zeeman manifold deriving from the situation that one atom is in an $m = +2$ state and the second one in an $m = +1$ state. The atomic projection quantum numbers lose their validity below distances of a few hundred Bohr radii, where atom-atom interactions become important.

nonadiabatic transitions to lower lying Zeeman states. Because of the steepness of the diabatically crossing channels, however, we do not expect severe losses and neglect them in this paper.

If one of the colliding atoms has $m = +2$ and the other one $m = +1$ at large distances, then $M_{\rm tot} = +3$ assuming $L = 0$. The final combination of two low-field seeking atoms—$m = +1$ for both atoms—corresponds to $M_{\rm tot} = +2$, again implying an s-wave collision. The two cases, $M_{\rm tot} = +3$ and $M_{\rm tot} = +2$, are shown in Figs. 2 and 3, respectively. The most dramatic difference between the cases $M_{\rm tot} = +4$ (Fig. 1) and $M_{\rm tot} = +3$ (Fig. 2) is the strength of the attractive potential an s-wave experiences: For $M_{\rm tot} = +3$, this is stronger by about one order of magnitude. In this Zeeman manifold the couplings are so strong that even a state correlating to a higher partial wave is subject to strong attractive forces. In Fig. 3, $M_{\rm tot} = +2$, the potential energy curves are even more complicated and suggest interesting cold-collision dynamics. There is a double degeneracy in this energy region at large interatomic separations, since two atoms with $m = +1$ have the same energy as one atom with $m = +2$ plus a second atom with $m = 0$. The latter atom cannot be magnetically trapped.

In the following we are going to concentrate on the long-range potential well in the energetically highest Zeeman manifold with $M_{\rm tot} = +4$ (Fig. 1). Molecular rotations are found to play a key role in its origin. We have calculated adiabatic potential energy curves for three different rotational basis set sizes and extracted those curves that correlate to two fully polarized strontium atoms in a rotational s-wave state. The results are shown in Fig. 4. If in addition to s-waves only d-waves are included—$L_{\rm max} = 2$—the potential energy curve is purely attractive (the same holds true if a pure s-wave basis is used). Only as soon as g-waves are taken into account ($L_{\rm max} = 4$) is there an effective repulsion below $R = 150$, thus leading to the emergence of a potential well minimum at large $R$. Nevertheless, the structure of the curve is still not converged. The potential energy curve obtained using $L_{\rm max} = 8$ illustrates the need for i- and k-waves. Larger rotational basis sets make it difficult to isolate a smooth potential energy curve due to the appearance of pronounced avoided crossings (see Fig. 1). However, the structure of the effective diabatic curve correlating at large distances to an s-wave is essentially the one found for $L_{\rm max} = 8$.

Deeper insight into the formation of the long-range potential well and the role played by molecular rotations can be gained by resorting to a perturbative approach. For that purpose we take the diagonal of the matrix $\boldsymbol{V}$ defined in Eq. (66) to represent the unperturbed problem; the perturbation is given by the off-diagonal elements. At large interatomic separations the state vector of two fully polarized metastable strontium atoms in a rotational s-wave state reads

$$\begin{aligned} |J_{\rm tot}, M_{\rm tot}, L, J\rangle &= |4, 4, 0, 4\rangle \\ &=: |\Phi_0\rangle\,. \end{aligned} \tag{67}$$

Up to first order its energy is

$$\langle\Phi_0|V|\Phi_0\rangle = -\frac{C_{6,0}}{R^6} - 2\,\langle\mu\rangle\,\mathcal{B}, \tag{68}$$

where $C_{6,0} = 5.33 \times 10^3$ a.u. Hence we see that the long-range attraction in the s-wave channel is entirely due to dispersion forces; more precisely, it derives from the scalar tensor $\boldsymbol{T}_0$ (see Eqs. (33), (58), and (59)).

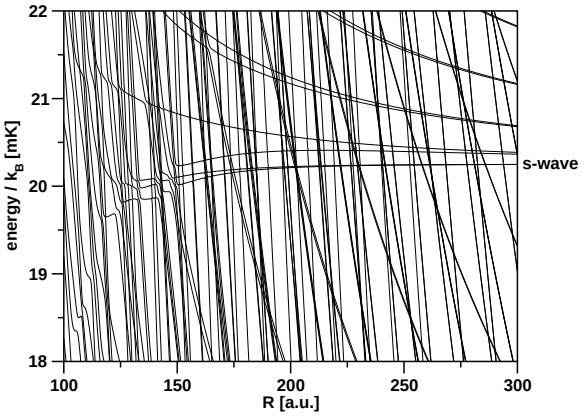


FIG. 3: Adiabatic potential energy curves of two metastable strontium atoms ((5s5p) $^3P_2$) in a magnetic field of 100 G, calculated setting $M_{\rm tot}$ to +2. Here, the focus is on the Zeeman manifold that correlates to two atoms with $m = +1$.

In order to evaluate the second-order correction, all basis vectors must be determined that can couple directly to $|\Phi_0\rangle$. Since $|\Phi_0\rangle$ is an eigenvector of both the rotational kinetic energy operator and the Zeeman operator, the coupling must be mediated by the anisotropic interatomic interaction. $H_{\rm I}$ preserves $J_{\rm tot}$ and couples $|\Phi_0\rangle$ to the basis vectors

$$\begin{aligned} |\Phi_1\rangle &:= |4,4,2,2\rangle\,, \\ |\Phi_2\rangle &:= |4,4,2,4\rangle\,, \\ |\Phi_3\rangle &:= |4,4,4,0\rangle\,, \\ |\Phi_4\rangle &:= |4,4,4,2\rangle\,, \\ |\Phi_5\rangle &:= |4,4,4,4\rangle\,. \end{aligned} \tag{69}$$

The first two are rotational d-waves, the other three are g-waves. Their first-order energies, together with that of $|\Phi_0\rangle$, are depicted in Fig. 5. Note that the basis vectors $|J_{\rm tot}, M_{\rm tot}, L, J\rangle$ are eigenvectors of the Zeeman operator only if $L$ or $J$ vanishes. Therefore, the long-range limits of the first-order energies do not in general agree with the Zeeman energies of two noninteracting atoms. In view of Fig. 5 it is tempting to conclude that the strong repulsion that gives rise to the molecular potential well is due to the d-wave $|\Phi_2\rangle$, whose energy comes close to and eventually crosses the energy of the s-wave channel.

However, this is not true. In Fig. 6 we have plotted the modulus squared of the coupling matrix elements $\langle\Phi_i|\,V\,|\Phi_0\rangle$, $i = 1, ..., 5$. Note the use of a logarithmic scale along the ordinate. The coupling of the s-wave to the g-waves $|\Phi_3\rangle$, $|\Phi_4\rangle$, and $|\Phi_5\rangle$ turns out to be stronger by many orders of magnitude than the coupling to the d-waves $|\Phi_1\rangle$ and $|\Phi_2\rangle$. The reason is the tensorial structure of $H_{\rm I}$ (Eqs. (33) and (55)): The d-waves couple to $|\Phi_0\rangle$ through the relatively weak second-rank tensor $\boldsymbol{T}_2$; the g-waves, however, couple to the s-wave via the fourth-rank tensor $\boldsymbol{T}_4$, which is dominated by the strong electric quadrupole-quadrupole interaction. Because $|\Phi_5\rangle$ is closest in energy to $|\Phi_0\rangle$ (Fig. 5) and its coupling matrix element is by far the greatest (Fig. 6), it is likely that it accounts for most of the second-order correction to the s-wave energy. Figure 7 confirms this. The difference between the full second-order energy and that due to $|\Phi_5\rangle$ alone is relatively small. What is even more important is the difference to the first-order energy. In first order, the s-wave experiences pure attraction by scalar dispersion forces. As a consequence of strong quadrupole-quadrupole coupling to g-waves associated with energetically lower Zeeman manifolds, a steep repulsive potential wall appears. This requires that coupling is introduced at least to second order in perturbation theory.

The simple perturbative approach does not provide quantitative agreement with our numerical results, but it evidently captures the basic physics underlying the existence of the long-range potential well. Moreover, it predicts that the properties of the potential well depend on $\mathcal{B}$, the magnetic-field strength. The energy difference between $|\Phi_0\rangle$ and the most important g-wave, $|\Phi_5\rangle$, is approximately independent of interatomic distance (Fig. 5). This can be exploited for a compact approximate representation of the second-order energy of $|\Phi_0\rangle$, valid at magnetic fields of about 100 G and higher:

$$\begin{aligned} E \;=\; & -2\,\langle\mu\rangle\,\mathcal{B} \\ & -\frac{C_{6,0}}{R^6} - \frac{1}{\langle\mu\rangle\,\mathcal{B}}\frac{\kappa}{R^{10}}. \end{aligned} \tag{70}$$

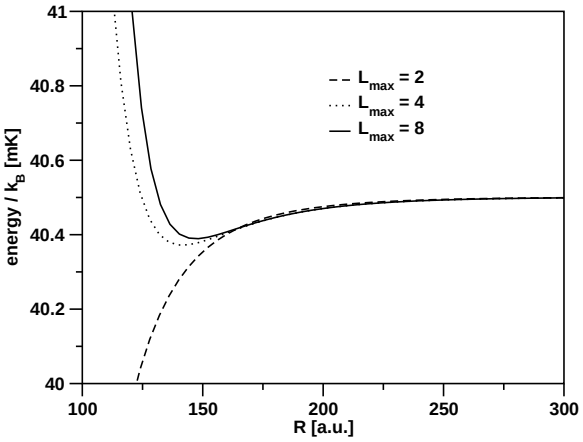


FIG. 4: Dependence of the potential energy curve of the "s-wave" in Fig. 1 on the largest molecular rotation quantum number, $L_{\max}$, taken into account in the construction of the matrix $\boldsymbol{V}$ (Eq. (66)). Only if g-waves are included does a potential well appear. The cause of the pronounced admixture of higher partial waves is the relatively strong, anisotropic quadrupole-quadrupole interaction. At large $R$, the curves converge to 40.502 mK, corresponding to the Zeeman energy of two metastable strontium atoms with $m = +2$ in a magnetic field of 100 G.

The quadrupole-quadrupole coupling parameter $\kappa$ is $1.44 \times 10^5$ a.u. The location, with respect to $R$, of the potential well minimum described by Eq. (70) scales as $\mathcal{B}^{-1/4}$, while the well depth scales as $\mathcal{B}^{3/2}$. As the magnetic-field strength is increased, the effect of electric quadrupole-quadrupole coupling at a given distance $R$ diminishes. In order to compensate for the larger Zeeman splittings, it is necessary to go to shorter distances. Along the way the dispersion attraction grows stronger, until it is eventually overwhelmed by repulsion induced by electric quadrupole-quadrupole interaction. The potential well therefore gets deeper and its minimum is shifted to smaller interatomic distances as $\mathcal{B}$ is ramped up.

The tunability of the molecular potential well could prove useful for controlling the properties of metastable, magnetically trapped $^{88}$Sr. The most important quantity in this context is the scattering length $a$ [48], which characterizes the effective interaction between ultracold collision partners [60]. A positive $a$ describes effective repulsion; negative $a$ implies attraction. The strength of the interaction is governed by $|a|$.

We have therefore calculated the scattering length in the long-range potential well as a function of magnetic-field strength, $\mathcal{B}$. Our results are displayed in Fig. 8. For each $\mathcal{B}$ value, we determined, in a procedure similar to the one that led to Fig. 4, the maximum $L$ that gave a smooth potential energy curve compatible with the respective result for $L_{\max} = 40$, but which no longer exhibits pronounced avoided crossings. We then numerically integrated the one-dimensional Schrödinger equation with the selected potential energy curve and for asymptotically vanishing kinetic energy from $R_{\min} = 40$ to $R_{\max} = 1940$ a.u. The scattering length was obtained from the logarithmic derivative of the computed wavefunction at $R = R_{\max}$. We verified that our results are converged with respect to variations of the integration limits $R_{\min}$ and $R_{\max}$.

We have restricted the lowest magnetic-field strength in Fig. 8 to $\mathcal{B} = 10$ G, because below that the potential well starts to disappear. At $\mathcal{B} = 0$, the long-range potential is purely attractive, and additional knowledge about the short-range part of the potential would be necessary in order to make quantitative predictions. The strongest field we have considered is $\mathcal{B} = 500$ G. The left classical turning point at this field strength is already down to about $R = 80$. Still higher field strengths would again maneuver us into a regime where our theory probably becomes unreliable (see the discussion at the beginning of this subsection). However, between 10 and 500 Gauss—and within the approximation of pure elastic scattering—our scattering lengths may be regarded as accurate to within about 10%.

There are two important features about the $\mathcal{B}$-dependence. First, the scattering length vanishes at $\mathcal{B}_0 = 173$ G. The slope at this point is $a'(\mathcal{B}_0) = -0.98/\text{G}$. Second, $a$ diverges at the resonance field strength $\mathcal{B}_{\text{res}} = 339$ G, which signals the appearance of the first bound state in the long-range potential well. In the vicinity of both $\mathcal{B}_0$ and $\mathcal{B}_{\text{res}}$ the effective interatomic interaction can be switched between attraction and repulsion. Near $\mathcal{B}_{\text{res}}$, the ability to tune $a$ over an extensive range may be particularly advantageous.

Interestingly, $\mathcal{B}_{\text{res}}$ and $\mathcal{B}_0$ are not independent of one another. We can derive an approximate analytic formula for

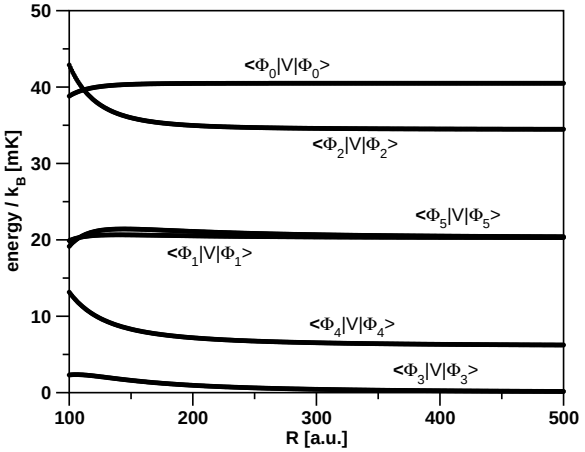


FIG. 5: Energy expectation values of the s-wave $|\Phi_0\rangle$ (Eq. (67)) and the five basis states that can couple directly to it (Eq. (69)). $|\Phi_1\rangle$ and $|\Phi_2\rangle$ are d-waves; $|\Phi_3\rangle$, $|\Phi_4\rangle$, and $|\Phi_5\rangle$ are g-waves.

the scattering length as a function of magnetic-field strength:

$$a(\mathcal{B}) = -\frac{8}{5\pi} a'(\mathcal{B}_0)\mathcal{B}_0 \times \left[1 - \tan\left(\frac{5\pi}{8}\sqrt{\mathcal{B}/\mathcal{B}_0} - \frac{3\pi}{8}\right)\right], \tag{71}$$

which depends only on the parameters $\mathcal{B}_0$ and $a'(\mathcal{B}_0)$. Equation (71) is based on a semiclassical analysis by Gribakin and Flambaum [61]. We have employed their analytic result for a hard-core plus a $1/R^n$-potential. In our case, the attraction is basically due to pure dispersion interaction and the repulsion is so strong that replacing it by a hard core is not such a bad approximation. In accordance with the discussion following Eq. (70), we assumed the onset of the hard core to scale as $\mathcal{B}^{-1/4}$. The first resonance in Eq. (71) appears when the argument of the tan-function equals $\pi/2$, or $\mathcal{B}/\mathcal{B}_0 = (7/5)^2 = 1.96$. This is in excellent agreement with our numerical data: $\mathcal{B}_{\rm res}/\mathcal{B}_0 = 339/173 = 1.96$. The scattering length as predicted by Eq. (71), using the parameters $\mathcal{B}_0 = 173$ G and $a'(\mathcal{B}_0) = -0.98/\text{G}$ estimated from our numerical data, is also plotted in Fig. 8. The analytic formula reproduces the magnetic-field dependence of the scattering length remarkably well.

## V. CONCLUSION

Potential wells associated with ordinary molecular bonds are typically a few electron volts, or $10^4$ Kelvin, deep; the minimum of the potential energy is found at interatomic distances of the order of one Bohr radius. Electronic interactions at such short distances are so strong that the energy separation between the ground and excited electronic states dissociating to the same atomic configuration is very large in comparison to rotational energies. In a simplified picture we might envisage the strong chemical bond as forcing the atoms into a fixed orientation with respect to the interatomic axis. Molecular rotation leaves this rigid arrangement virtually unaffected.

In fact, however, the long-range physics of metastable alkaline-earth atoms is fundamentally different from that simplistic picture. If the atoms are separated by a sufficiently large distance, they have constant angular momenta. As the atoms approach one another, they experience anisotropic forces that modify the molecular rotational motion as well as the relative orientation of the nonspherical atoms. At interatomic distances of a few hundred Bohr radii, the energy scales of interatomic interactions and molecular rotations are comparable, and the coupling between atomic and molecular angular momentum turns out to be rather efficient.

The tensorial analysis presented in this paper puts the coupling mechanism into a particularly clear and useful form. Our formulation makes maximum use of symmetries, which allows a compact matrix representation of the long-range Hamiltonian. It will enable systematic multichannel scattering calculations needed to investigate the role played by inelastic collision processes.

In this study we have numerically diagonalized the Hamiltonian matrix for two metastable strontium atoms and obtained adiabatic potential energy curves, the adiabaticity referring only to the *distance* coordinate $R$. The curves are in general very complicated. We have therefore focussed on one curve—associated with an s-wave channel and with

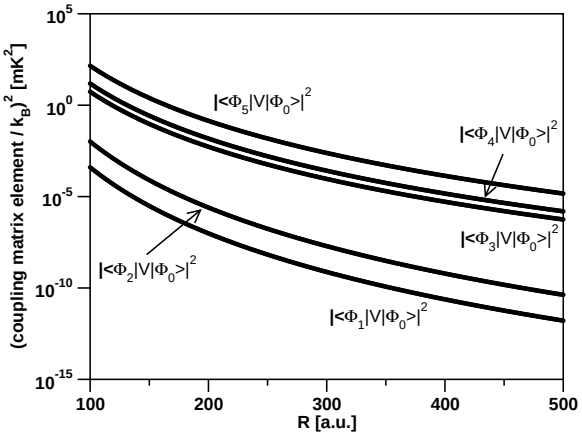


FIG. 6: Coupling strengths of the basis states $|\Phi_1\rangle$ through $|\Phi_5\rangle$ (Eq. (69)) to the s-wave $|\Phi_0\rangle$ (Eq. (67)), plotted on a logarithmic scale. The coupling increases rapidly as the interatomic distance is reduced. It is strongest for the g-waves $|\Phi_3\rangle$, $|\Phi_4\rangle$, and $|\Phi_5\rangle$, which can couple to $|\Phi_0\rangle$ via electric quadrupole-quadrupole interaction. The coupling of $|\Phi_0\rangle$ to the d-waves $|\Phi_1\rangle$ and $|\Phi_2\rangle$ is mediated by the comparatively weak dispersion interaction.

the atoms in an experimentally attractive low-field seeking state—that exhibits a novel type of long-range potential well. This well arises from a fascinating interplay between the pure $1/R^6$-attraction in the s-wave channel and the strong quadrupole-quadrupole coupling to rotational g-waves attached to lower lying Zeeman manifolds. Recently, Avdeenkov and Bohn discovered that the anisotropic forces between polar OH molecules in an electrostatic field lead to a similar phenomenon [62].

The scattering length in the long-range potential well in metastable strontium can be tuned by varying the external magnetic-field strength. We find a resonance at 339 G, which differs quantitatively from the prediction by Derevianko *et al.* [25], who estimate the resonance location to lie near 1000 G. We believe that the present calculations should improve upon the accuracy of the more approximate treatment of Ref. [25].

Finally, the nature of the resonance deserves attention. It indicates the emergence of the first vibrational bound state as the long-range potential well undergoes a controlled deformation. This process must be contrasted with the physics underlying Feshbach resonances [63, 64, 65, 66], where the scattering wave in the entrance channel is brought into resonance with a vibrational bound state in a potential well correlating to an energetically higher channel. The potential energy curves themselves do not change their qualitative appearance. The strong anisotropic interactions in cold gases of metastable alkaline-earth atoms open an entirely new route to shaping potential energy curves and creating temporary molecules with bond lengths of the order of a hundred Bohr radii.

### Acknowledgments

We would like to thank Kevin Christ for contributing his one-electron finite-element code. We thank Hossein Sadeghpour and Andrei Derevianko for discussions. R.S. gratefully acknowledges financial support by the Emmy Noether program of the German Research Foundation (DFG). This work was supported in part by the Department of Energy, Office of Science.

[1] J. O. Hirschfelder, C. F. Curtiss, and R. B. Bird, *Molecular Theory of Gases and Liquids* (Wiley, New York, 1964).
[2] E. A. Cornell and C. E. Wieman, Rev. Mod. Phys. **74**, 875 (2002).
[3] W. Ketterle, Rev. Mod. Phys. **74**, 1131 (2002).
[4] J. Weiner, V. S. Bagnato, S. Zilio, and P. S. Julienne, Rev. Mod. Phys. **71**, 1 (1999).
[5] M. Marinescu, H. R. Sadeghpour, and A. Dalgarno, Phys. Rev. A **49**, 982 (1994).
[6] M. Marinescu, J. F. Babb, and A. Dalgarno, Phys. Rev. A **50**, 3096 (1994).
[7] S. H. Patil and K. T. Tang, J. Chem. Phys. **106**, 2298 (1997).
[8] A. Derevianko, W. R. Johnson, M. S. Safronova, and J. F. Babb, Phys. Rev. Lett. **82**, 3589 (1999).
[9] M.-K. Chen, J. Phys. B **28**, 4189 (1995).
[10] Z.-C. Yan and J. F. Babb, Phys. Rev. A **58**, 1247 (1998).

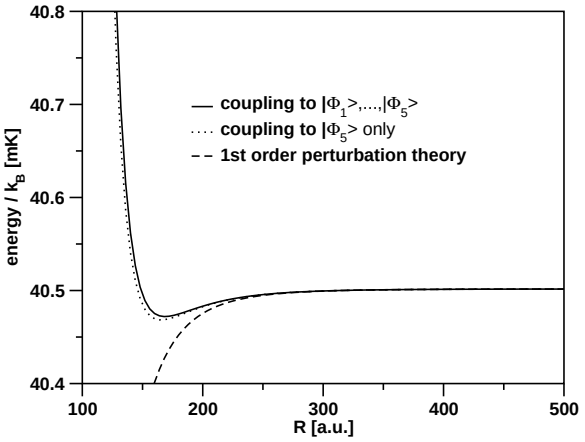


FIG. 7: In first-order perturbation theory, the potential energy curve of the s-wave $|\Phi_0\rangle$ is purely attractive (Eq. (68)). Due to the strong coupling to the g-waves, in particular $|\Phi_5\rangle$, a potential well emerges. An approximate analytic representation is given in Eq. (70).


[11] A. Derevianko and A. Dalgarno, Phys. Rev. A **62**, 062501 (2000).
[12] M. R. Doery, E. J. D. Vredenbregt, S. S. Op de Beek, H. C. W. Beijerink, and B. J. Verhaar, Phys. Rev. A **58**, 3673 (1998).
[13] T. P. Dinneen, K. R. Vogel, E. Arimondo, J. L. Hall, and A. Gallagher, Phys. Rev. A **59**, 1216 (1999).
[14] X. Xu, T. H. Loftus, M. J. Smith, J. L. Hall, A. Gallagher, and J. Ye, Phys. Rev. A **66**, 011401(R) (2002).
[15] H. Katori, T. Ido, Y. Isoya, and M. Kuwata-Gonokami, Phys. Rev. Lett. **82**, 1116 (1999).
[16] M. Machholm, P. S. Julienne, and K.-A. Suominen, Phys. Rev. A **64**, 033425 (2001).
[17] G. Zinner, T. Binnewies, F. Riehle, and E. Tiemann, Phys. Rev. Lett. **85**, 2292 (2000).
[18] T. Loftus, J. R. Bochinski, and T. W. Mossberg, Phys. Rev. A **63**, 053401 (2001).
[19] T. Loftus, J. R. Bochinski, and T. W. Mossberg, Phys. Rev. A **66**, 013411 (2002).
[20] A. Derevianko, Phys. Rev. Lett. **87**, 023002 (2001).
[21] H. Katori, T. Ido, Y. Isoya, and M. Kuwata-Gonokami, in *Atomic Physics* **17**, edited by E. Arimondo, P. DeNatale, and M. Inguscio (AIP, Melville, NY, 2001).
[22] S. B. Nagel, C. E. Simien, S. Laha, P. Gupta, V. S. Ashoka, and T. C. Killian, Phys. Rev. A **67**, 011401(R) (2003).
[23] X.-Y. Xu, T. H. Loftus, J. L. Hall, A. Gallagher, and J. Ye, J. Opt. Soc. Am. B , in press (May 1, 2003).
[24] P. E. Siska, Rev. Mod. Phys. **65**, 337 (1993).
[25] A. Derevianko, S. G. Porsev, S. Kotochigova, E. Tiesinga, and P. S. Julienne, Phys. Rev. Lett. **90**, 063002 (2003).
[26] P. E. S. Wormer, F. Mulder, and A. van der Avoird, Int. J. Quant. Chem. **11**, 959 (1977).
[27] R. P. Leavitt, J. Chem. Phys. **72**, 3472 (1980); erratum in J. Chem. Phys. **73**, 2017 (1980).
[28] P. Piecuch, Int. J. Quant. Chem. **25**, 449 (1984).
[29] B. Zygelman, Phys. Rev. Lett. **64**, 256 (1990).
[30] W. Clark and C. H. Greene, Rev. Mod. Phys. **71**, 821 (1999).
[31] A. R. Edmonds, *Angular Momentum in Quantum Mechanics* (Princeton University Press, Princeton, 1957).
[32] U. Fano and G. Racah, *Irreducible Tensorial Sets* (Academic Press, New York, 1959).
[33] R. N. Zare, *Angular Momentum: Understanding Spatial Aspects in Chemistry and Physics* (Wiley, New York, 1988).
[34] J. D. Jackson, *Classical Electrodynamics* (Wiley, New York, 1998).
[35] H. Margenau, Rev. Mod. Phys. **11**, 1 (1939).
[36] A. Dalgarno and W. D. Davison, in *Adv. At. Mol. Phys.* **2**, edited by D. R. Bates and I. Estermann (Academic Press, New York, 1966).
[37] T. Y. Chang, Rev. Mod. Phys. **39**, 911 (1967).
[38] W. J. Meath, J. Chem. Phys. **45**, 4519 (1966).
[39] M. E. Rose, *Elementary Theory of Angular Momentum* (Dover, New York, 1995).
[40] H. Feshbach, Ann. Phys. (N.Y.) **5**, 357 (1958).
[41] H. Feshbach, Ann. Phys. (N.Y.) **19**, 287 (1962).
[42] U. Fano and J. H. Macek, Rev. Mod. Phys. **45**, 553 (1973).
[43] C. H. Greene and R. N. Zare, Ann. Rev. Phys. Chem. **33**, 119 (1982).
[44] C. H. Greene and R. N. Zare, J. Chem. Phys. **78**, 6741 (1983).
[45] G. Racah, Phys. Rev. **61**, 186 (1942).
[46] G. Racah, Phys. Rev. **62**, 438 (1942).
[47] G. Racah, Phys. Rev. **63**, 367 (1943).
[48] J. J. Sakurai, *Modern Quantum Mechanics* (Addison-Wesley, Reading, 1994).
[49] D. A. Varshalovich, A. N. Moscalev, and V. K. Khersonsky, *Quantum Theory of Angular Momentum* (World Scientific, Singapore, 1988).

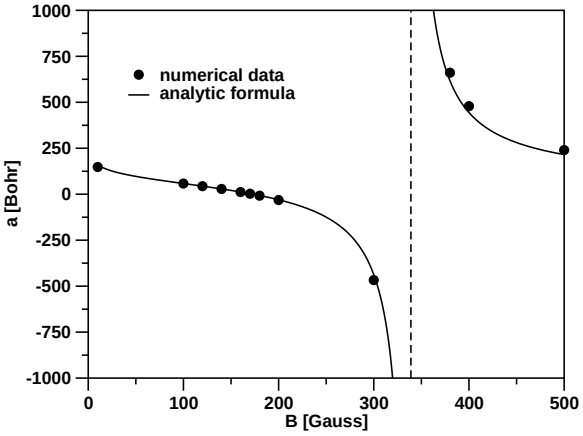


FIG. 8: Scattering length, $a$, in the long-range potential well calculated as a function of the magnetic-field strength, $\mathcal{B}$. The dots represent numerical data obtained by direct integration of the one-dimensional Schrödinger equation. The solid line is based on the analytic formula in Eq. (71) ($\mathcal{B}_0 = 173$ G and $a'(\mathcal{B}_0) = -0.98/\mathrm{G}$).


[50] Z.-C. Yan, J. F. Babb, A. Dalgarno, and G. W. F. Drake, Phys. Rev. A **54**, 2824 (1996).
[51] T. Bergeman, G. Erez, and H. J. Metcalf, Phys. Rev. A **35**, 1535 (1987).
[52] G. Audi and A. H. Wapstra, Nucl. Phys. A **565**, 1 (1993).
[53] M. Aymar, C. H. Greene, and E. Luc-Koenig, Rev. Mod. Phys. **68**, 1015 (1996).
[54] W. R. Johnson, D. Kolb, and K.-N. Huang, At. Data Nucl. Data Tables **28**, 333 (1983).
[55] E. U. Condon and G. H. Shortley, *The Theory of Atomic Spectra* (Cambridge University Press, London, 1967).
[56] C. H. Greene, Phys. Rev. A **42**, 1405 (1990).
[57] M. Braun, W. Schweizer, and H. Herold, Phys. Rev. A **48**, 1916 (1993).
[58] J. Ackermann and J. Shertzer, Phys. Rev. A **54**, 365 (1996).
[59] K. W. Meyer, C. H. Greene, and B. D. Esry, Phys. Rev. Lett. **78**, 4902 (1997).
[60] C. J. Pethick and H. Smith, *Bose-Einstein Condensation in Dilute Gases* (Cambridge University Press, Cambridge, 2002).
[61] G. F. Gribakin and V. V. Flambaum, Phys. Rev. A **48**, 546 (1993).
[62] A. V. Avdeenkov and J. L. Bohn, Phys. Rev. A **66**, 052718 (2002).
[63] S. Inouye, M. R. Andrews, J. Stenger, H.-J. Miesner, D. M. Stamper-Kurn, and W. Ketterle, Nature **392**, 151 (1998).
[64] Ph. Courteille, R. S. Freeland, D. J. Heinzen, F. A. van Abeelen, and B. J. Verhaar, Phys. Rev. Lett. **81**, 69 (1998).
[65] J. L. Roberts, N. R. Claussen, J. P. Burke, Jr., C. H. Greene, E. A. Cornell, and C. E. Wieman, Phys. Rev. Lett. **81**, 5109 (1998).
[66] S. L. Cornish, N. R. Claussen, J. L. Roberts, E. A. Cornell, and C. E. Wieman, Phys. Rev. Lett. **85**, 1795 (2000).